Supporting Information

Oxygen-deficient TiO_2 and carbon coupling synergistically boost Ru nanoparticles for alkaline hydrogen evolution reaction

Zhongzhe Wei[a], Zijiang Zhao[a], Jing Wang[b,*], Qiang Zhou[a], Chenxia Zhao[a], Zihao Yao[a], Jianguo Wang[a,*]

E-Mail: jgw@zjut.edu.cn

[a]Institute of Industrial Catalysis, College of Chemical Engineering, Zhejiang University of Technology, Hangzhou 310032, P. R. China.

[b] Institute of Advanced Magnetic Materials, College of Materials and Environmental Engineering, Hangzhou Dianzi University, Hangzhou, Zhejiang 310018, P. R. China.

Table S1. The element analysis results for different catalysts.

Sample	C (%)	H (%)	Ru (%)
Ru/TiO_2@C-0	0.08	0.43	-
Ru/TiO_2-V_O@C-5	7.00	0	3.2
Ru/TiO_2-V_O@C-10	12.17	0.77	3.0
Ru/TiO_2-V_O@C-15	13.58	0.97	2.9
Ru/TiO_2-V_O@C-20	14.33	1.02	2.8

Table S2. Summary of the recently reported noble metal-based HER catalysts.

Catalyst	η-j[a]	Electrolyte solution	Reference
Ru/TiO_2-V_O@C-15	64-10	1.0 M KOH	This work
R-TiO_2:Ru (5%)	150-10	0.1 M KOH	*J. Am. Chem. Soc.*, 140 (2018), 5719
Ru/C_3N_4/C	79-10	0.1 M KOH	*J. Am. Chem. Soc.*, 138 (2016), 16174
Cu_{2-x}@Ru	82-10	1.0 M KOH	*Small*, 13 (2017), 1700052
Ru_{SA}-N-S-$Ti_3C_2T_x$	76-10	0.5 M H_2SO_4	*Adv. Mater.*, 31 (2019), 1903841
ECM@Ru	63-10	0.5 M H_2SO_4	*Adv. Energy Mater.*, 10 (2020), 2000882
Sr_2RuO_4	61-10	1.0 M KOH	*Nat. Commun.*, 10 (2019), 149
Ni-doped RuO_2 NWs	52-10	1.0 M KOH	*J. Mater. Chem. A*, 7 (2019), 6411
RuS_x/S–GO	58-10	1.0 M KOH	*Small*, 15 (2019), 1904043
Ru0.33Se@TNA	57-10	1.0 M KOH	*Small*, 14 (2018), 1802132
hydrous RuO_2	60-10	1.0 M KOH	*Chem. Phys. Lett.*, 673 (2017), 89-92
Pt-Ru-Mo	196-10	Seawater	*J. Mater. Chem. A.*, 4 (2016), 6513
Pt@2D-Ni(OH)$_2$	123-4.2	0.1 M KOH	*Nano Energy*, 31 (2017), 456

Ru/SiNWs	200-10	0.5 M H_2SO_4	*Electrochem. Commun.*, 52 (2015), 29
Ru-CNT	63-4.874	0.5 M H_2SO_4	*Int. J. Hydrogen Energy*, 41 (2016), 23007
RuP_2@NPC	52-10	1.0 M KOH	*Angew. Chem., Int. Ed.*, 56 (2017), 11559
GCE-S-CNs-1000-CB-Ru	~80-10	0.5 M H_2SO_4	*Carbon* 93 (2015), 762

[a] η represents the overpotential calculated at the current density of j (j/mA cm^{-2}).

Table S3. H_2 chemisorption results for different Ru/TiO_2-Vo@C catalysts.

Sample	**H_2 uptake ($mmol_{H2}$ g_{Ru}^{-1})**
Ru/TiO_2-Vo@C-5	0.273
Ru/TiO_2-Vo@C-10	0.338
Ru/TiO_2-Vo@C-15	0.394
Ru/TiO_2-Vo@C-20	0.356

Table S4. The EPR semi-quantitative analysis results for different catalysts.

Sample	Amount of oxygen vacancies (spins/g)
Ru/TiO_2-V_O@C-5	$1.436*10^{18}$
Ru/TiO_2-V_O@C-10	$6.928*10^{18}$
Ru/TiO_2-V_O@C-15	$8.462*10^{18}$
Ru/TiO_2-V_O@C-20	$7.665 *10^{18}$
Ru/TiO_2-V_O@C-25	$1.561*10^{15}$
Ru/TiO_2-V_O@C-15-800 °C	$8.355*10^{16}$

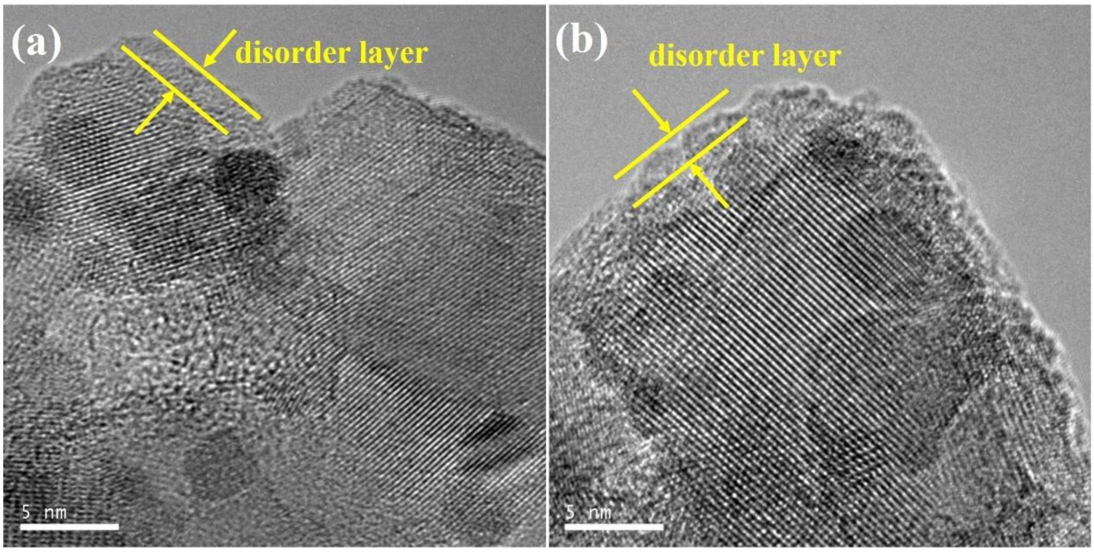

Figure S1. HRTEM images of Ru/TiO_2-Vo@C-15 to show the oxygen vacancies on TiO_2.

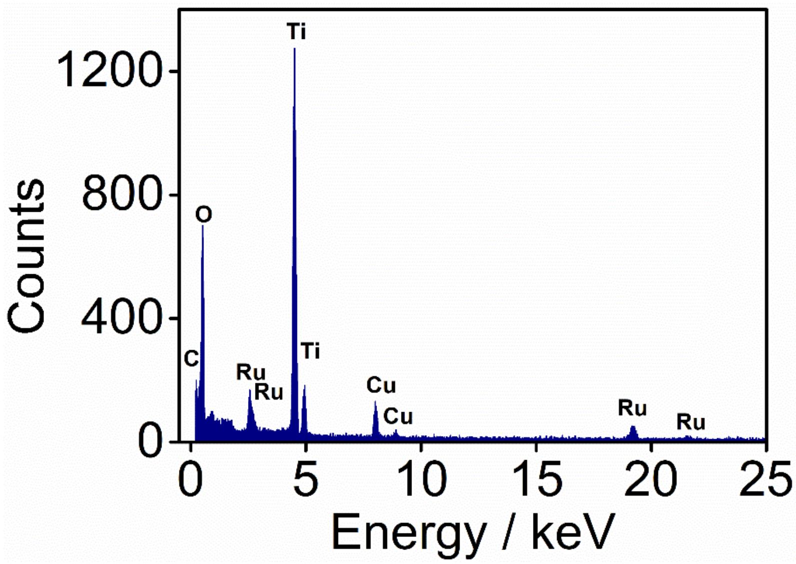

Figure S2. The energy dispersive X-ray (EDX) spectrum of Ru/TiO_2-V_O@C-15.

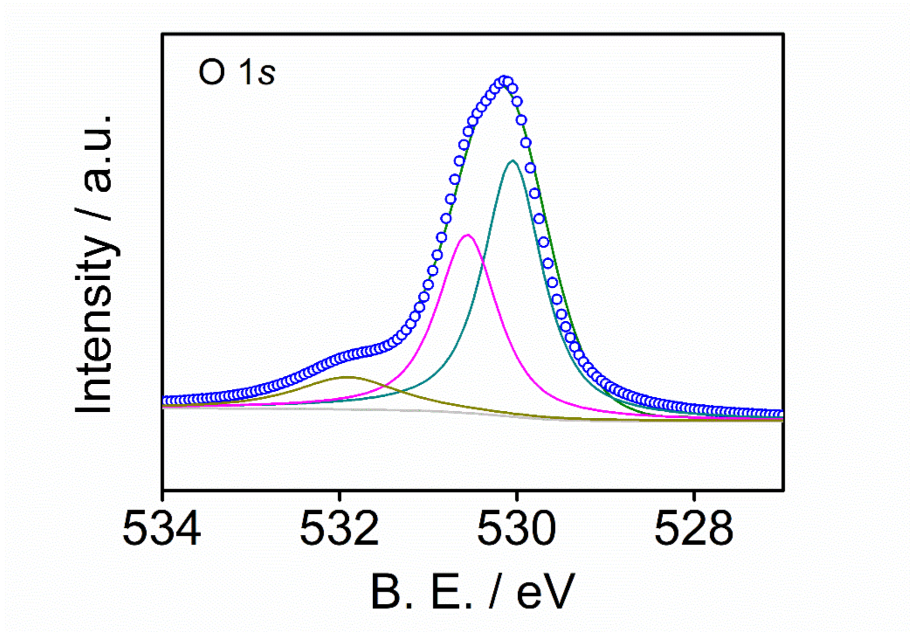

Figure S3. O 1s XPS spectrum for Ru/TiO_2-V_O@C-15.

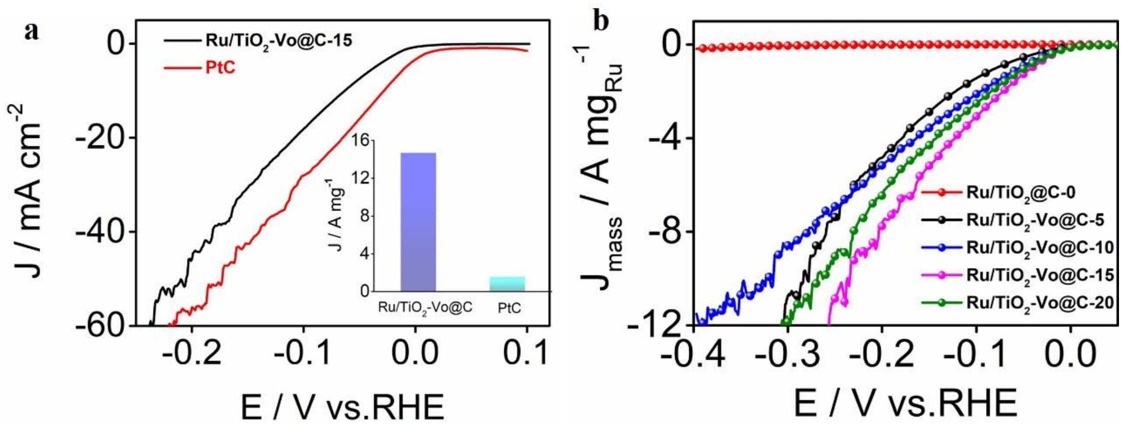

Figure S4. (a) Polarization curves of Ru/TiO_2-V_O@C-15 and Pt/C in 1 M KOH. The inset shows the mass activity of Ru/TiO_2-V_O@C-15 and Pt/C at an overpotential of -300 mV (vs reversible hydrogen electrode, RHE). (b)The mass activities of the catalysts (normalized the currents by Ru contents).

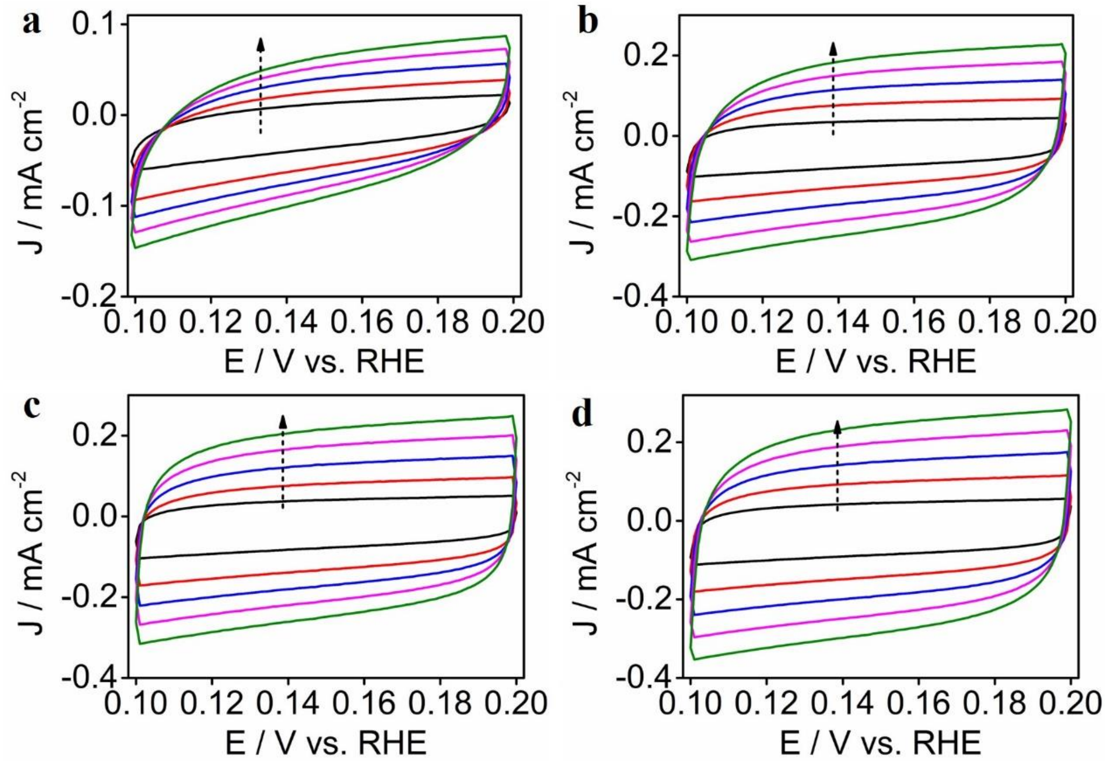

Figure S5. Cyclic voltammetry curves of (a) Ru/TiO2-V_O@C-5, (b) Ru/TiO2-V_O@C-10, (c) Ru/TiO2-V_O@C-15 and (d) Ru/TiO2-V_O@C-20, respectively. The arrow indicates the scan rate from 10 mV to 50 mV.

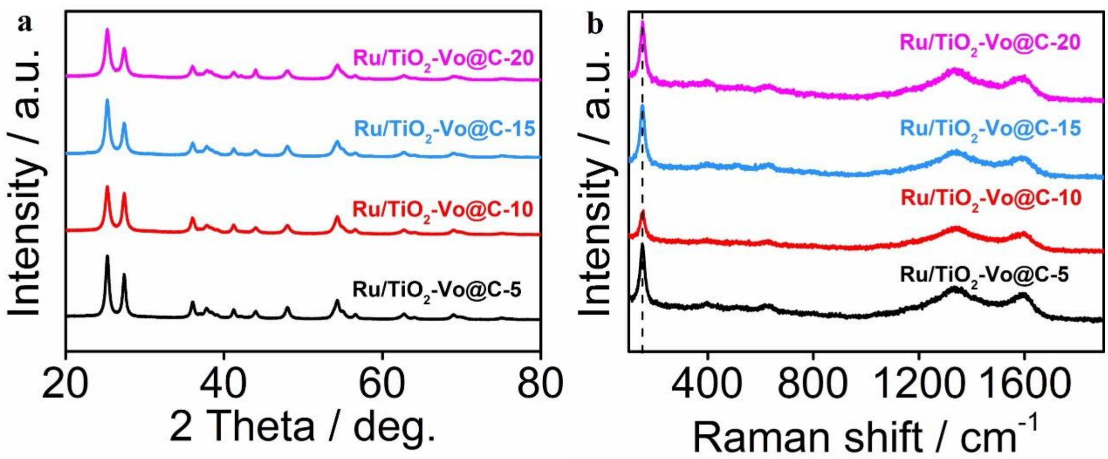

Figure S6. XRD and Raman patterns of Ru/TiO2-Vo@C-X (X = 5, 10, 15 and 20).

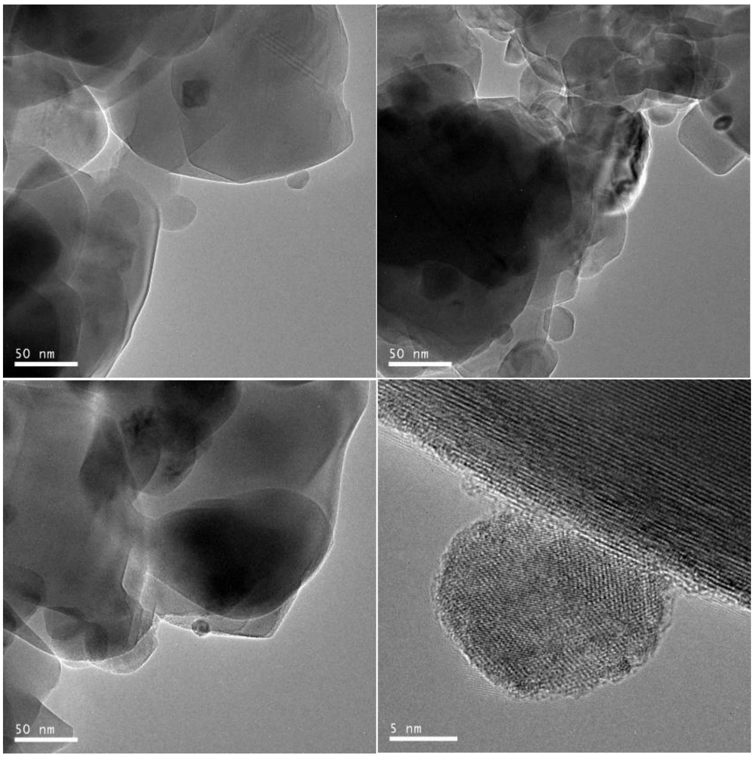

Figure S7. Represented TEM and HRTEM images of Ru/TiO_2@C-0.

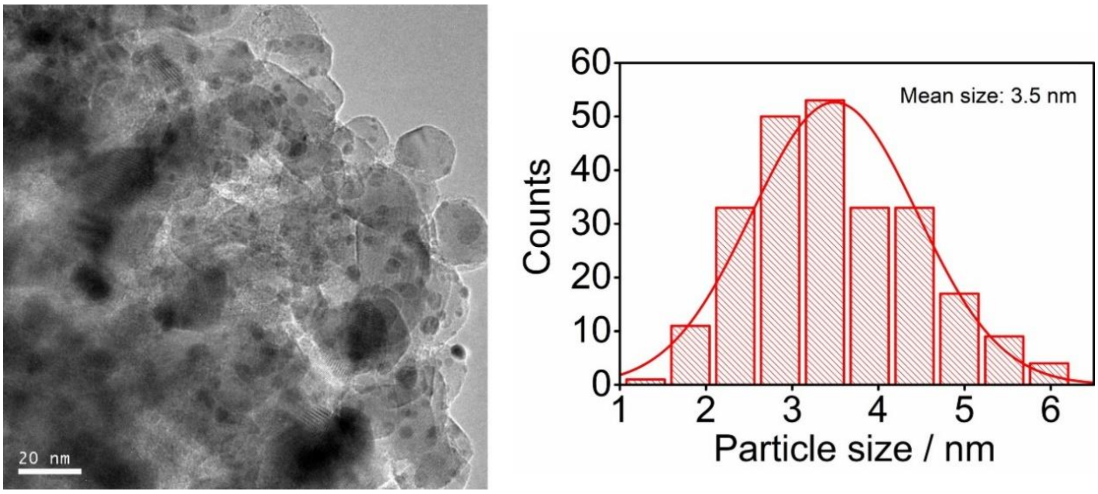

Figure S8. TEM image and corresponding Ru particle size distribution histogram of Ru/TiO_2-Vo@C-5.

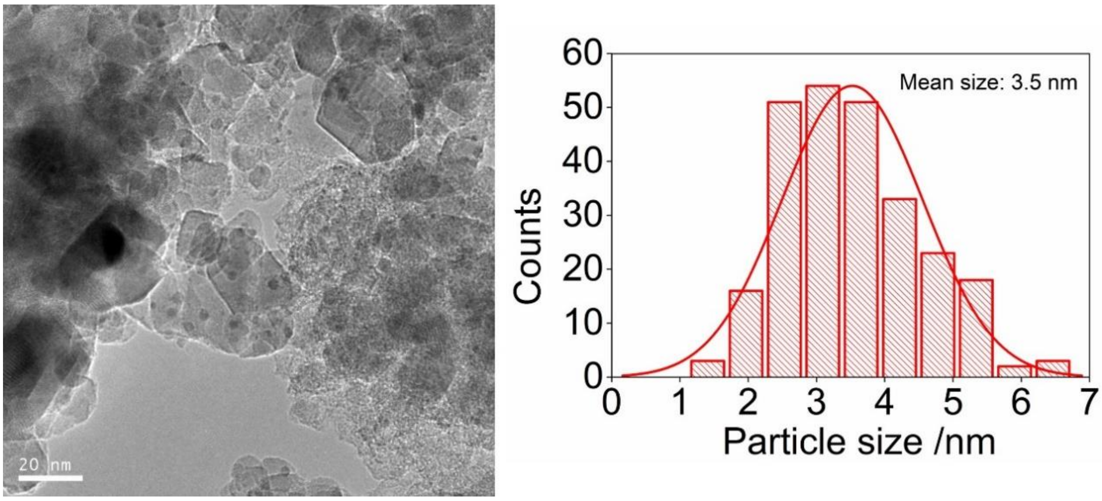

Figure S9. TEM image and corresponding Ru particle size distribution histogram of Ru/TiO_2-Vo@C-10.

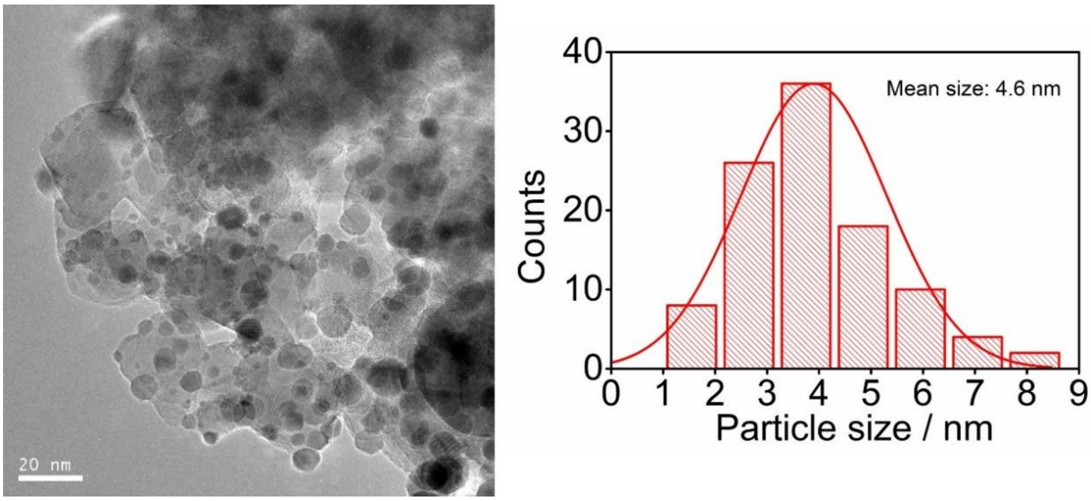

Figure S10. TEM image and corresponding Ru particle size distribution histogram of Ru/TiO_2-Vo@C-20.

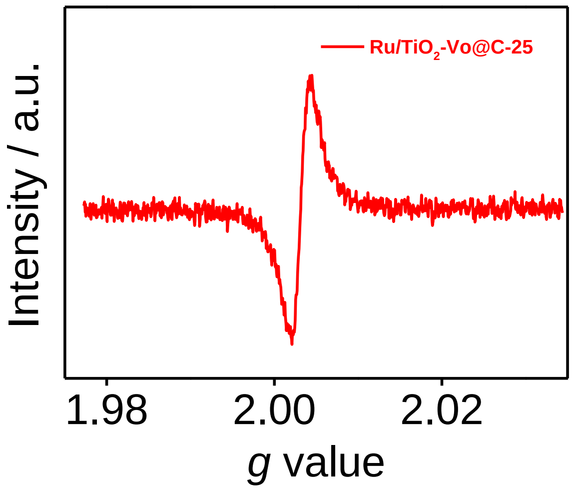

Figure S11. EPR signal of Ru/TiO_2-V_O@C-25.

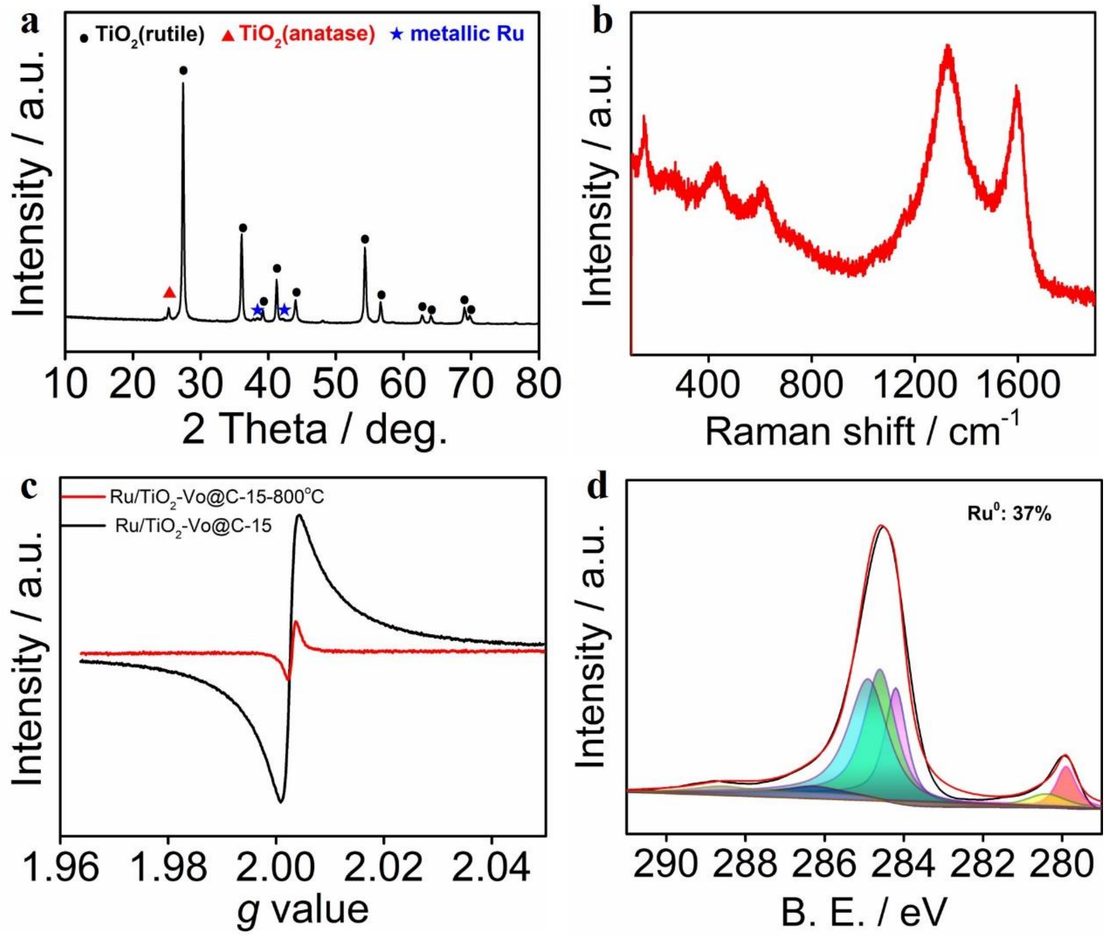

Figure S12. (a) XRD pattern, (b) Raman spectrum, (c) EPR spectra, and (d) Ru 3d XPS spectrum of Ru/TiO_2-V_O@C-15-800 ºC.

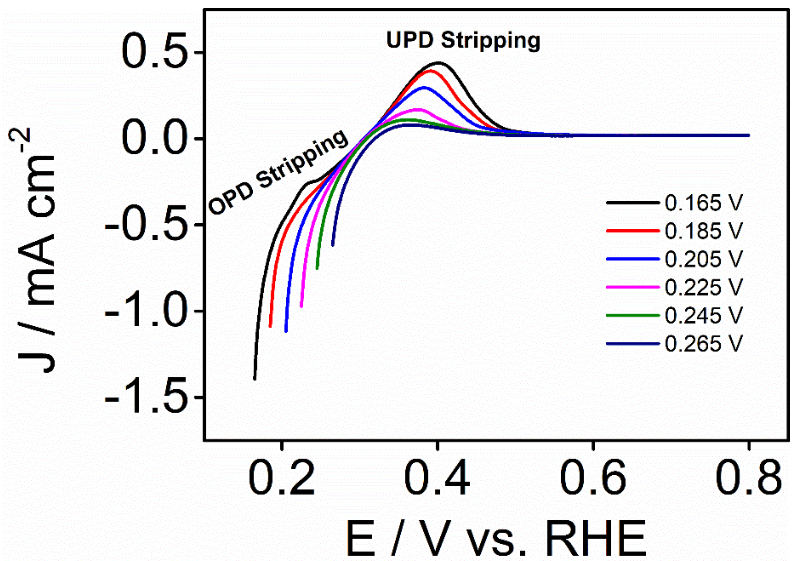

Figure S13. LSV curves of Ru/TiO_2-V_O@C-15 under different initial voltages.

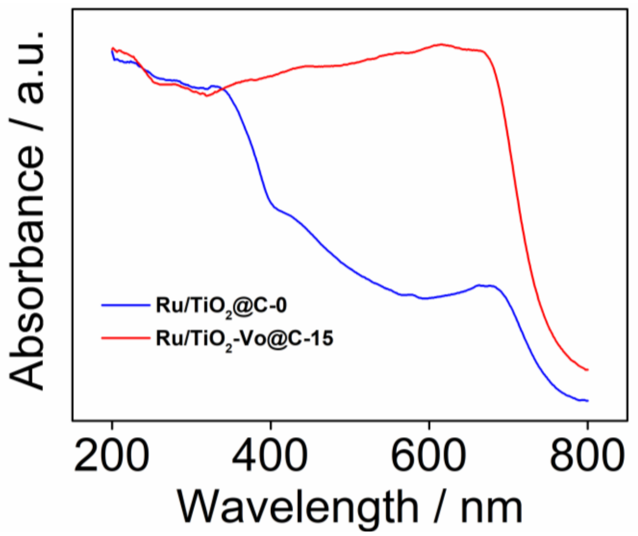

Figure S14. Diffuse reflectance UV-vis spectrum of Ru/TiO_2-V_O@C-15 and Ru/TiO_2@C-0.

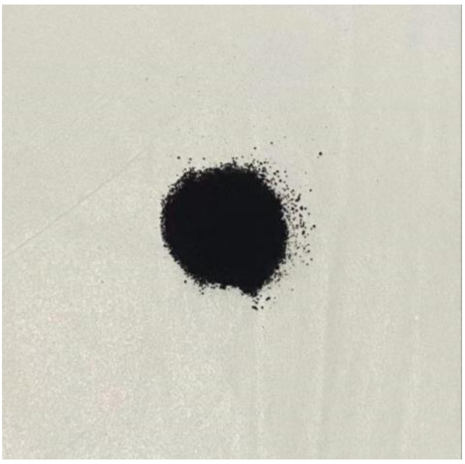

Figure S15. Optical image for Ru/TiO_2-V_O@C-15.

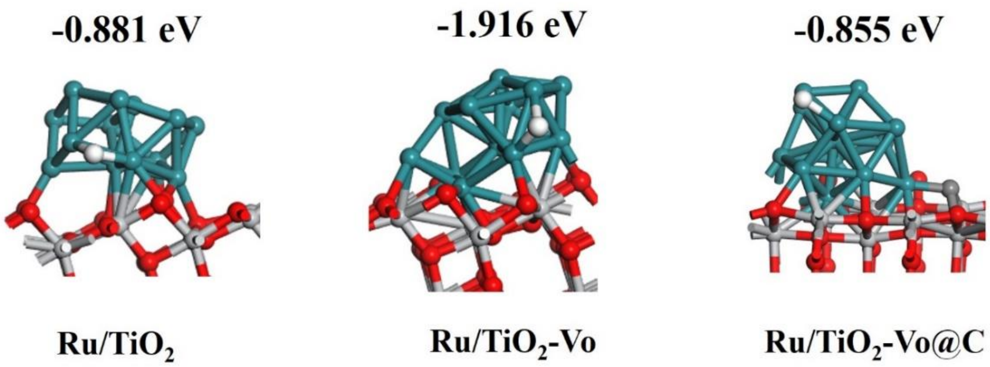

Figure S16. The H* adsorption energies of Ru/TiO_2, Ru/TiO_2-Vo and Ru/TiO_2-Vo@C and corresponding structures.